Coulomb-correlated few-electron states in a transmission electron microscope beam

Rudolf Haindl,[1,2] Armin Feist,[1,2,*] Till Domröse,[1,2] Marcel Möller,[1,2] Sergey V. Yalunin,[1,2] and Claus Ropers[1,2,†]

[1] *Max Planck Institute for Multidisciplinary Sciences, D-37077 Göttingen, Germany*
[2] *4th Physical Institute - Solids and Nanostructures, Georg-August-Universität Göttingen, D-37077 Göttingen, Germany*

We observe Coulomb-correlated electron pair and triple states generated by femtosecond photoemission from a nanoscale field emitter inside a transmission electron microscope. Event-based electron spectroscopy allows for spatial and spectral characterization of the electrons emitted by each laser pulse. Distinctive energy and momentum correlations of two- and three-electron states are identified, revealing a strong few-body Coulomb interaction at an energy scale of about two electronvolts. State-sorted beam caustics show a discrete increase in virtual source size and longitudinal source shift for few-electron states, associated with transverse momentum correlations. The pronounced spatial and spectral characteristics of these electron number states allow for filtering schemes that control the statistical distribution of the pulse charge. In this way, the fraction of specific few-electron states can be actively suppressed or enhanced, facilitating the preparation of highly non-Poissonian electron beams for microscopy and lithography, including future schemes in correlated two-electron probing.

Correlations between electrons are at the core of numerous phenomena in atomic, molecular, and solid-state physics. Mediated by the Coulomb force, few- and many-body electronic correlations govern intriguing phases of matter, such as superconductivity or charge ordering, and they underpin a wide variety of applications, down to nanoscale logic gates based on single charges. In contrast to the opportunities granted by electron correlations in condensed matter, in the case of free-electron beams, Coumlomb interaction between electrons is typically considered a detrimental factor. In electron microscopy, electron repulsion leads to stochastic longitudinal and transverse emittance growth of the beam, described by the Boersch [1, 2] and Loeffler [3] effects, respectively, and limiting the brightness of state-of-the-art electron sources [4, 5]. In high-charge electron pulses for time-resolved experiments, space-charge effects govern the achievable pulse duration, energy spread and focusability [6], and pose a major experimental challenge for ultrafast electron diffraction [7–11] and microscopy [6, 12, 13], particle accelerators [14] and free-electron lasers [15].

Studying strong electronic correlations for a beam containing only few particles requires the preparation of a high electron phase space degeneracy. Field emitters represent highly localized sources, and they have been used in studies elucidating free-electron correlations [16–18] involving exchange-mediated [17] and Coulomb [19] interactions. Short-pulsed laser excitation of such nanotip sources can further confine the emission in time [20–27], for use in ultrafast electron microscopy and diffraction with high-coherence beams [11, 13, 28]. The pulse-averaged effects of Coulomb interactions from such sources have recently been investigated, associated with spectral broadening and a loss of temporal and spatial resolutions [6, 29–32].

Correlations among free electrons have previously been identified using coincidence detection, employing concepts from atomic and molecular science for measuring electrons and ions [33, 34] as well as correlated photoemission [35, 36] and ionization [37, 38]. In electron microscopy, the recent advent of pixelated event detectors has substantially widened the capabilities for coincidence measurements involving electrons, as demonstrated for electron-correlated X-ray emission [39], cathodoluminescence at nanomaterials [40] and integrated photonic resonators [41]. These capabilities will foster the emerging area of free-electron quantum optics, promising quantum coherent manipulation [42–47] and sensing [48, 49] at the nanoscale, and facilitating concepts based on electron-electron [16, 50, 51] or electron-light entanglement [41, 50, 52]. Establishing such schemes will require a fundamental understanding of correlations within the single electrons constituting the beam.

Here, we demonstrate strong Coulomb correlations in two-electron and three-electron states generated at a laser-driven Schottky field emitter. Using event-based electron spectroscopy and imaging, kinetic energy distributions of electron ensembles emitted by single laser pulses are recorded, sorting events by the number of free electrons. Characteristic double- and triple-lobe spectra for events containing two and three electrons, respectively, are found. We quantitatively characterize interparticle correlations in both energy and transverse momentum, and observe that stochastic few-body interactions dominate over mean-field (space charge) effects. Two-particle energy correlation functions reveal a pronounced peak around 1.7 eV energy difference, illustrating an effective joint emission area for electron pair-states far smaller than the physical and virtual source sizes. These observations strongly suggest a coherent one-step process for two-electron-two-photon emission reminiscent of strongly correlated double-electron emission from atomic systems or solids. The findings shed light on fundamental correlations in multi-electron emission, and enable statistical control of electron beams for on-demand correlated few-particle imaging and spectroscopy.

The experiments presented in this study were carried

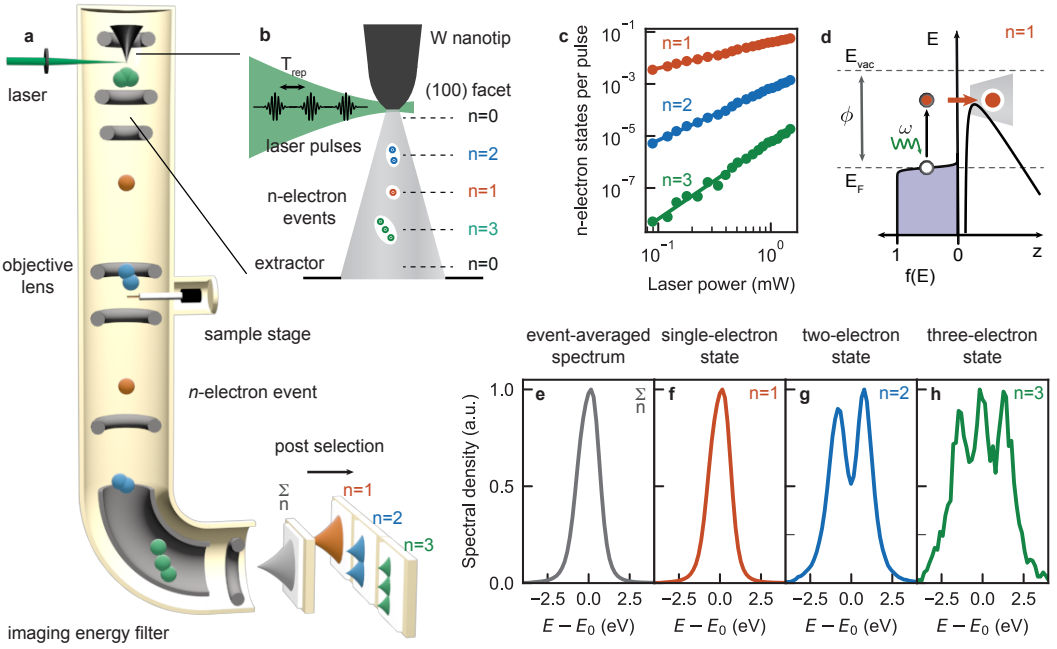

Figure 1. **Coulomb-correlated few-electron states in a transmission electron microscope. a,** Experimental setup. Few electron-states are prepared by pulsed photoemission. The electrons pass the sample plane of the microscope, and post selection in event-based electron spectroscopy enables number state selective beam analysis. **b,** Ultrashort electron pulses are emitted from a laser-assisted Schottky field emitter (W(110)/ZrO_x nanotip), with a pulse charge up to few electrons coupled to the microscope column. **c,** Power-scaling of the rates of one-, two- and three-electron states. The bunching ratios for the double-/triple-electron states are $r_2 = 0.85$ and $r_3 = 0.57$, respectively (see text). **d,** Schematic of one-photon laser-assisted near-threshold Schottky emission. **e,** The event-averaged spectrum is separated into number-state resolved contributions ($n = 1, 2, 3$, **f-h**). The two- and three-electron spectra show a distinct shape with n peaks, indicating a discrete energetic separation of the contained electrons.

out at the Göttingen Ultrafast Transmission Electron Microscope (see sketch in Fig. 1a) [13]. Using a femtosecond laser source, ultrashort electron pulse trains at low pulse charge are generated by near-threshold laser-assisted Schottky emission from a W(100)/ZrO_x emitter. After propagation through the column of the microscope, the electrons are detected with an event-based camera. The temporal resolution of the electron detector allows to discriminate between consecutive incident electron pulses, providing an unambiguous measure of the number n of transmitted electrons per laser pulse (see Fig. 1a,b).

The rates of n-electron events as a function of incident laser power are displayed in Fig. 1c. Specifically, the rate of single-electron emission scales linearly with power, in agreement with the employed process of near-threshold laser-assisted Schottky photoemission [13, 53] (see Fig. 1d). In turn, he $n = 2$- and $n = 3$-electron rates scale according to the power of n, i.e., with the square and cube, respectively, of the laser power.

Considering the relative distribution of n-electron events at a given laser power, we identify weakly sub-Poissonian statistics. Specifically, defining P_n as the probability to detect n electrons in a pulse, a Poisson process predicts a probability distribution of $P_n = r_n P_1^n/n!$ with $r_n = 1$. The actual rates measured for $n \geq 2$ are somewhat lower, corresponding to bunching ratios of $r_2 = 0.85$ and $r_3 = 0.57$, respectively. This confirms moderate antibunching of few-electron states, as recently observed from different field emitters for the case of $n = 2$ [16–18].

We next investigate the kinetic energies of these number-sorted electron states (Figs. 1e-h). The spectral distribution of the one-electron events (f), which also dominates the total spectrum (e, summed over all events), consists of a single peak centered around the acceleration voltage of $E_0 = 200\,\mathrm{keV}$. In stark contrast, the spectra of the two- and three-electron events (g,h) exhibit a pronounced double- and triple-lobe structure, respectively, with a mean energy at E_0.

Beyond this average over similar events, our measurement scheme further allows us to link the spectral characteristics to two- and three-particle correlations within individual electron pulses. Figure 2a shows the pair-density distribution as a function of the electron energies E_A and E_B associated with two electrons A and B in the same electron pulse. The pair density shows a strong correlation in the form of an energy gap around zero energy difference $E_A - E_B$. This strong correlation proves that the observed splitting of the $n = 2$ spectrum into a double-lobed structure is the result of a two-electron Coulomb interaction, which we further investigate below.

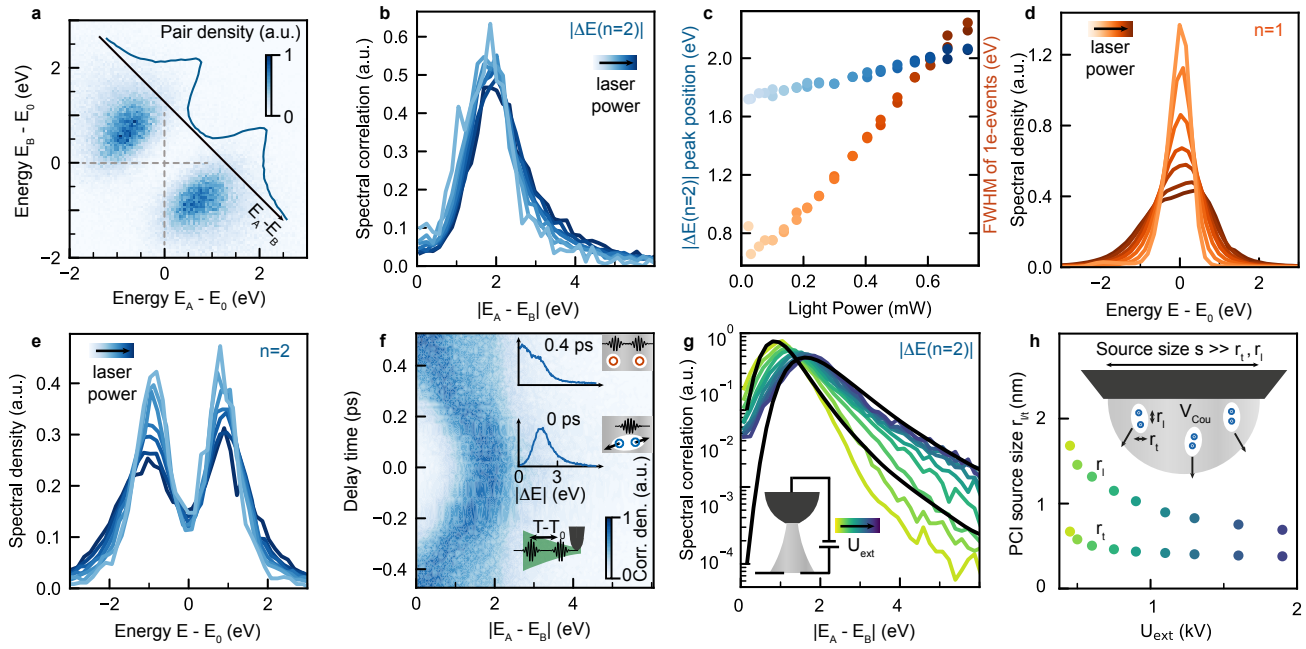

Figure 2. **Strongly correlated electron pair-states. a,** Energy histogram of coincident electron pairs revealing a strong correlation in relative kinetic energy, visible in the spectral correlation function (inset, integrated along the diagonal). **b,** Normalized one-sided pair correlation functions ($n = 2$) for varying laser power. **c,** Power scaling of the peak position of the $n = 2$-correlation function compared to the spectral width (FWHM) of the $n = 1$-state (spectra shown in panel **d**). **e,** Normalized n=2-spectra for varying laser power. **f,** Pair correlation function for photoemission with two delayed laser pulses. In temporal overlap, a strong correlation gap is observed, disappearing for ≈200 fs pulse delay (see cross sections as inset). **g,** Extraction voltage U_{ext} dependent spectral correlation function (solid lines: fitted spectral distribution). **h,** Transverse (r_{tra}) and longitudinal (r_{lon}) dimensions of the extracted interparticle distances from panel **g** (inset: illustration comparing correlation volume with virtual source size).

Similar to a conventional (not laser-triggered) Schottky source, only a fraction of electrons generated at the emitter surface is transmitted into the microscope column [6]. Consequently, mean-field (space charge) as well as stochastic interactions with random nearby electrons not entering the beam need to be considered and distinguished from the correlation observed in the electron pair state. Laser-power-dependent measurements allow for an assessment of these different contributions. The corresponding $n = 1$ and $n = 2$ (Figs. 2d,e) spectral distributions exhibit a broadening with increasing laser power (cf. Fig.2c, orange circles), i.e. with average photocurrent. This is in close correspondence to previous non-event-selective measurements [2, 6, 31] and is typically ascribed to stochastic Coulomb interactions and mean-field effects.

In contrast, the set of two-electron correlation functions displayed in Fig. 2b is remarkably independent of laser power, showing a pronounced gap that is about 1 eV wide, a peak at around 1.8 eV, and an extended tail towards large energy separations exceeding 4 eV. Increasing the photocurrent only imposes moderate variations in the depth of the gap and the shape of the high-energy tail. In particular, the position of the main correlation peak (Fig. 2c, blue circles) approaches a fixed value of 1.7 eV towards vanishing laser power, i.e. small average currents. This demonstrates that the observed correlation is only weakly altered by multiple Coulomb interactions with aperture-blocked electrons, and that it is dominated by the two-electron correlation alone.

In order to investigate the temporal extent over which such strong Coulomb correlations prevent the generation of independent single electrons, we conducted measurements using a pair of laser pulses of variable delay (see Fig. 2f) and at constant integrated laser power. Two different ranges are identified: Temporally overlapping laser pulses reproduce the described $n = 2$ correlation function. In contrast, a temporal separation of more than 200 fs coincides with a significantly reduced energy difference, indicative of electron pairs containing two uncorrelated electron emission events.

Whereas there is only weak dependence of the correlation on emission current, we found that the extraction field applied to the tip has a more prominent influence. A decrease in extraction voltage substantially changes the observed gap and the slope of the high-energy tail (see semilogarithmic plot in Fig. 2g). Physically, a change in extraction voltage affects the height of the Schottky barrier, the acceptance angle of the beam and the virtual source size [54]. The spectral shapes of these correla-

tion functions can be modeled in a straightforward manner by an ensemble of electron doublets prepared with a Gaussian-distributed interparticle distance, and assuming that the initial Coulomb potential energy is eventually converted to relative kinetic energy. Using separate standard deviations r_{lon} and r_{tra} for the longitudinal (perpendicular to the surface) and transverse (parallel to the surface) distributions, respectively, this simple model successfully describes the main features of the measured correlation functions (cf. solid lines in Fig. 2g). Extracting the spatial parameters from fits of the model to the data (Fig. 2h), we obtain transverse and longitudinal dimensions of $r_{\mathrm{lon}} = 0.5 - 0.7$ nm and $r_{\mathrm{tra}} = 0.8 - 1.9$ nm, respectively, with a weak dependence of r_{tra} on extraction voltage and a continuous increase of r_{lon} for lower extraction fields.

These strikingly small spatial scales of less than one nanometer in interparticle distance highlight the strong correlations observed, but they must also be considered a surprise. The physical source size of the (100) emission plane of the Schottky field emitter (on the order of 100 nm [55]) as well as the backprojected virtual source size (around 20 nm [54]) are substantially larger than the projected 1 nm, from within the doublet electrons appear to stem. This implies a distinct two-electron emission channel, which directly leads to the emission of a highly-correlated electron pair state by joint two-photon absorption.

However, as the correlation function nearly vanishes at zero energy difference, it is evident that beyond such a two-electron emission channel, there are hardly any additional events containing two uncorrelated (or weaker-correlated) electrons. This is noteworthy, as the rate of Coulomb-correlated electron doublets amounts to 85 % of what is expected from a Poisson number distribution and the one-electron rate. The lack of 15 % of two-electron events (antibunching) could be attributed to local Coulomb blockade [56, 57], Pauli blocking [17], or transverse interparticle deflection and spatial filtering.

In other words, the statistical occurrence frequency of two-electron events is rather close to what would be expected from uncorrelated emission events from the extended nanoscale source, while the spectral distribution indicates a highly-correlated two-electron emission process. This is to be contrasted with previously observed one-photon, two-electron emission processes [58], where the electron-pair emission channel is a subtle additional contribution to photoemission otherwise dominated by independent single-electron events.

A mechanism accounting for these observations must therefore predict both a practical absence of weakly correlated events, and a nearly Poissonian rate and two-photon scaling of strongly correlated pairs. At present, there is no established mechanism, such that we discuss possible contributions to the process. A straightforward explanation would be that, in fact, the effective emitter is only about 1 nm in diameter, possibly as a result of a specific adsorbate atop the ZrO layer, or a surface defect. We deem this a highly unlikely scenario, as we have observed the same correlations for different emitters, after multiple heating cycles, and over the course of months. Moreover, beam characterization does not indicate that the emitter leads to vastly improved spatial coherence over other Schottky emitters we studied in our laboratory, for which a much larger source size is known. Nonetheless, measurements on another emitter geometry or type could be carried out in the future.

In order to explain the prominence of electron pair emission, we note some mechanisms which were previously invoked in atomic and molecular contexts as well as two-electron photoemission. In atoms exposed to strong laser fields, enhanced "non-sequential" double ionization has been observed, initially in Helium [59] and subsequently in many other elements. Various mechanisms including co-tunneling, shake-up processes, and rescattering of a field-driven electron have been used to describe the observations, while the latter mechanism appears to be responsible in most cases [33, 34]. At the rather moderate local intensities in our experiments, the ponderomotive potential is significantly below 1 meV, such that recollision can be ruled out as a dominant factor. In the linear regime, one-photon two-electron emission is common in the Auger effect, where a core-hole resulting from photoemission is filled during the concurrent emission of a second electron. Coulomb interaction is a dominant factor in this process [60]. It is well known that for overlapping spectral distributions of the photoelectron and the Auger electron, the indistinguishable nature of the two electrons may enforce a coherent single-step process, governed by exchange interference in the final state and strong post-collision interaction, leading to a Coulomb splitting of the type observed here. Such a mechanism is

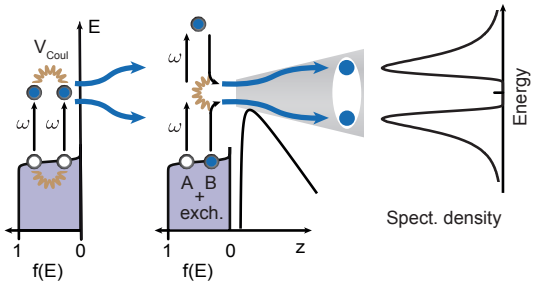

Figure 3. **Paths for Coulomb-correlated electron pair generation.** Two-photon two-electron emission can proceed via single-photon absorption by each electron, in conjunction with correlations in the initial and final states (left). Alternative diagrams involve a single-step coherent two-photon absorption path coupled to Auger-type Coulomb scattering, and leading to degenerate electron emission (center). Transformation of Coulomb energy to relative kinetic energy (sometimes called post-collision interaction) results in the gapped two-electron spectrum observed experimentally (sketch on the right). Indistinguishability of both electrons creates electron exchange terms and may facilitate quantum correlations and entanglement.

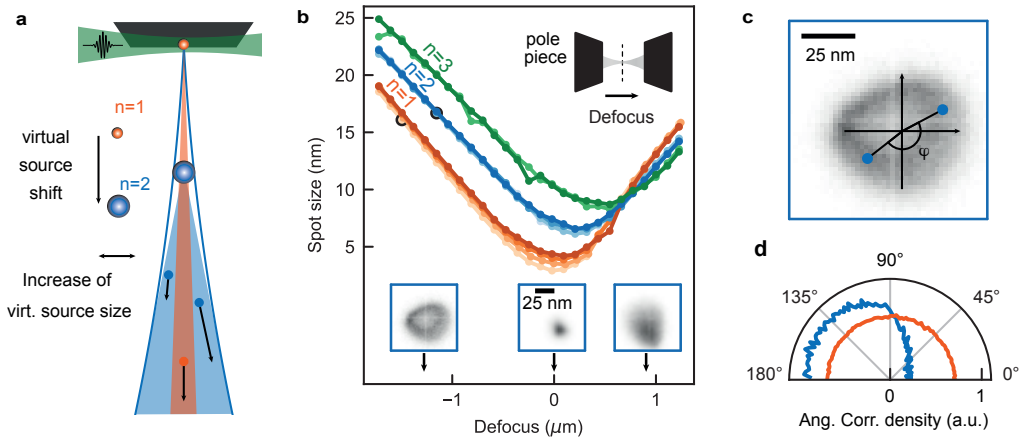

Figure 4. **Characterization of the spatial beam properties of few-electron states. a,** Schematic of the effect of Coulomb interaction. The virtual source increases in size and is shifted along the electron beam axis for pulse charges of two and three electrons. **b,** Caustics of the electron beam sorted by n, recorded by varying the last condenser lens of the microscope (low power: light color, high power: dark color). Insets: images of the beam profile for $n = 2$ in underfocus (left), focus (middle) and overfocus (right). **c,** Image of the beam profile in underfocus, and correlation angle φ between electron pairs with respect to the beam center. Long angle legs in the underfocus condition allow for a precise measurement of the angular correlation. **d,** A strong anisotropic angular correlation is observed for $n = 2$, compared to an isotropic distribution for drawing random events from the n=1 event class (employed data sets indicated in **b** by black circles around the data points).

not only established in atomic systems [61], but was analogously observed for resonant one-photon two-electron emission from a Cu(001) surface [58].

Figure 3 sketches several possible emission channels resulting in highly correlated electron pairs, involving either the absorption of one photon per electron (panel a) or Coulomb-mediated one-step double-electron emission involving a two-photon transition amplitude on one of the electrons (panel b). Generally, all intermediate paths leading to the same final state with indistinguishable, Coulomb-correlated electrons need to be coherently summed, together with diagrams including A/B exchange. Requiring Coulomb-scattering at high energies change, the latter process intrinsically involves strong correlations, but it is unclear how its total rate could amount to the observed value close to that of assumed uncorrelated emission events. Overall, the strong angular selection of the emission renders the microscopic emission site unresolvable in principle, such that correlation enhancements from small momentum differences may be relevant. The practical absence of weakly-correlated or uncorrelated emissions from different locations on the extended physical source remains a subject of further investigations, which could address specifics of exchange interference as well as material dependencies and initial-state correlations.

Alongside their spectral distributions and correlations, the few-electron states observed here possess characteristic spatial properties, discussed in the following. Specifically, in Fig. 4b, we measure n-dependent beam caustics, which exhibit discrete differences in both minimum spot size and focal position. Variations with laser power yield changes to the caustics (higher power leads to some increase in spot size), but are far less pronounced than the differences between the event classes. Under the given conditions, the focusability is limited by spherical aberration of the objective lens and the virtual source size, which result in typical spot profiles for positive and negative defocus (inset in Fig. 4b). Evidently, the $n \geq 1$ caustics are the result of a larger effective source, and the beam waist is shifted towards positive defocus.

Both observations can be understood from mutual transverse deflection sketched in Fig. 4a. Specifically, transverse deflection is expected to laterally spread the few-electron trajectories [6], such that the virtual source increases in size and moves forward, as predicted in simulations [32, 56].

A more detailed analysis of the spatial properties of few-electron states is obtained by analyzing correlations in transverse momentum. To this end, we measure position correlations for a sufficiently large negative defocus (Fig. 4c). The spatial correlation is quantified via the angle φ between the two electrons and the beam center. Figure 4d shows the angular correlation density of the two-electron state compared with random correlations drawn from a corresponding single-electron state at the same spot size (15 nm). In the electron pair state, we obtain a strong anisotropic correlation peaked around an angle of 180°, corresponding to electron events localized on opposite sides of the defocused beam, and thus having nearly opposite transverse momenta.

These observations show that averaging over number states has a severe impact on the beam properties, including non-correctable stochastic aberrations. A control of the number statistics in the photoemitted beam may thus directly benefit microscopy applications with such sources. More generally, stochastic Coulomb interactions are a fundamental issue in electron microscopy,

limiting electron source brightness via altering a beam's transverse (Loeffler) and longitudinal (Boersch) momentum distributions. The moderate antibunching observed here and in previous work [18] implies that the total photocurrent exhibits weakly sub-Poissonian noise characteristics, a property highly sought after in condensed matter scenarios (e.g. achieved by Coulomb blockade [62]). In the context of electron microscopy, this feature could be directly applied for shot-noise reduction in imaging, spectroscopy and lithography. However, perhaps even greater potential arises from the strong Coulomb-correlations in energy and momentum identified for the few-electron states. For example, the fact that both electrons in the doublet state are well-separated in energy and transverse momentum from each other allows for an energetic or spatial selection of the respective number state. This facilitates a powerful approach to control the statistics of single- and double electron events.

In particular, analyzing the measured spot profiles, a spatial aperture in a beam cross-over could be used to selectively favor the transmission T_1 of the $n = 1$ number state by a factor of 3 and nearly 8 over the transmissions T_2 and T_3 of the $n = 2$ and $n = 3$ states, respectively (Figs. 5a,b). Similarly, a pre-specimen energy filter commonly used in state-of-the-art electron microscopes [63] could be adjusted to enhance the transmission probability for $n = 1$ as compared to $n = 2$ states (see Fig. 5c). Specifically, for experimentally measured single-electron and double-electron spectra (Fig. 5e), the $n = 1$ transmission probability exceeds the $n = 2$ transmission probability by a factor of 8 at small slit widths, greatly amplifying the sub-Poissonian nature of the electron number distribution and facilitating a shot-noise-reduced electron current. Conversely, a central beam stop in energy can suppress a substantial fraction of single-electron states, leading to an up to 20-fold enhancement of pair-state over $n = 1$ state transmissions (see Fig. 5d,f). This approach will enable new forms of microscopy and spectroscopy with correlated electrons, for a variety of novel two-point or two-time measurement schemes in correlated materials and free-electron quantum optics.

In conclusion, the highly correlated few-electron states introduced in this work are of interest both for fundamental considerations, including the microscopic generation mechanism, and for their potential utility in manifold electron beam applications. For example, the pair state can be employed to implement a high-fidelity source of electron-heralded single-electrons, enabling shot-noise-free imaging and lithography with a precisely counted number of electrons. Furthermore, the elementary scattering process creating these well-defined few-body states may generally be assumed to induce entanglement between the electrons. Future studies may address the quantum coherence of such multi-electron states and their use as entangled free-electron qubits, with potential applicants spanning from interaction-free or correlation-based quantum electron microscopy to quantum information processing.

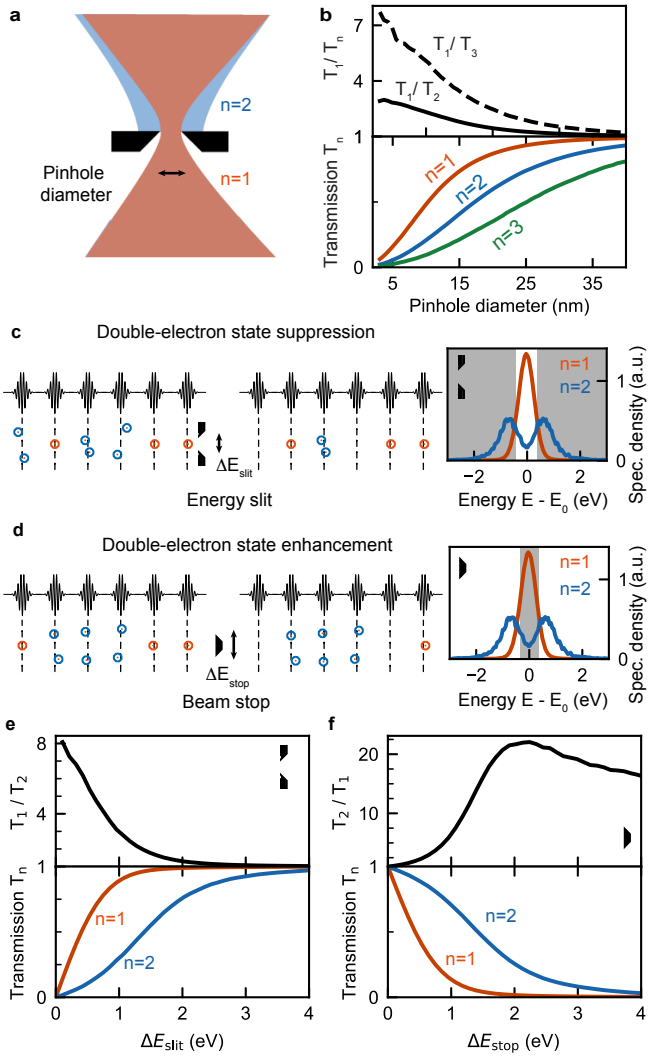

Figure 5. **Statistical control of single- and double-electron states using spatial and spectral filtering. a,** A pinhole positioned at the beam waist of the $n = 1$-beam profile spatially filters higher-number states. **b,** State-selective beam transmissions T_n (calculated from data in Fig. 4) and transmission ratios T_1 / T_2 and T_1 / T_3, with increased relative selectivity of the $n = 1$-electron state. **c,d,** In a spectrally dispersed plane, an energy-selective slit significantly reduces the transmission of $n = 2$-electron states. An energy beam stop suppresses the $n = 1$-electron states. Right: Experimental spectra of $n = 1$ and $n = 2$ electron states (gray area: spectral density rejected by energy slit/beam stop). **e,f)** Plot of the transmission T_n and transmission ratios T_1/T_2 and T_2/T_1, for the scenarios in **c** and **d**. Considering individually optimized energy windows, an 8-fold and 20-fold enhanced state-selectivity is found for $n = 1$ and $n = 2$, respectively.

In the final phase of manuscript preparation, we became aware of a related study by S. Meier, J. Heimerl and P. Hommelhoff.

METHODS

A. Femtosecond electron pulse generation in a transmission electron microscope

The experimental work was carried out in a commercially available transmission electron microscope (JEOL JEM 2100F) that has been modified to allow for the investigation of ultrafast dynamics in a stroboscopic laser-pump/electron-probe measurement scheme [13]. As our electron source, we employ a W/ZrO Schottky emitter (r = 490 nm radius-of-curvature) operated at an extraction voltage of U_{ext} = 2 kV and a bias voltage of $U_{\mathrm{bias}} = -0.3$ kV. Cooling the emitter just below the continuous Schottky-emission threshold of 1150 K (filament current 1.6 A), we generate ultrashort electron pulses via linear photoemission by focusing laser pulses (160 fs pulse duration, 515 nm central wavelength, 600 kHz repetition rate) onto the apex of the nanotip. While we estimate that every electron pulse initially consists of up to a few hundred electrons [6], apertures in the electro-optical beam path limit the transmitted beam to electrons that were generated close to the optical axis, resulting in average transmitted bunch charges of below one electron per pulse. Subsequent acceleration to 200 keV energy and coupling into the microscope column enable a pulse characterisation in real- and reciprocal space, spectral pulse properties are determined by an imaging energy filter (CEFID, CEOS GmbH).

B. Event-driven photoelectron detection

The photoelectron correlations experiments are imaged with a hybrid pixel electron detector that is based on the Timepix3 ASIC (EM CheeTah T3, Amsterdam Scientific Instruments B.V.) and mounted behind the energy filter. The camera generates a stream of data packages containing the position of electron-activated detector pixels, their time-of-arrival (ToA), which are digitized with 1.56 ns time bins, and the energy (time-over-threshold, ToT) associated with incident electron events. At a beam voltage of 200 kV every individual electron activates a cluster of pixels with variable size ($N_{\mathrm{pixels,avg}} \approx 8$ pixels), shape and energy ($\mathrm{ToT}_{\mathrm{avg}} \approx 280$ a.u.).

Single-electron event localisation of the ToT-corrected raw data stream is achieved using the Division of Nanoscopy, M4I, Maastricht University event clustering code [64], which is based on a Hierarchical Density-Based Spatial Clustering (HDBSCAN) in Python3. The algorithm reconstructs the timing and position of individual electrons incident on the detector from the activated pixels. Thereby, individual electrons are distinguished in terms of their ToA, attributing between three and nine neighbouring pixels activated within a time window of 100 ns and a summed ToT ranging from from 200 a.u. to 400 a.u. to the same cluster (see Ref. [65]).

In a second step, the photoelectrons are clustered according to the femtosecond laser pulse that generated them. The temporal resolution of the detector (1.56 ns) is much faster than the temporal pulse separation given by the laser repetition rate ($\approx$ 1 µs), but much slower than the temporal splitting of the correlated electrons at the detector ($\approx$ 1 ps). Hereby, the electrons arriving at the detector within Δt_{n} =50 ns are assigned to a number-class electron state $n = 1, 2, 3, ...$ determined by the number of electrons in one laser pulse.

C. Double Laser-pulse electron generation

For the two-laser-pulse generation described in Fig. 2f, a Michelson interferometer splits the incoming laser pulse into two separate pulses. One of the interference arms has a variable optical path length, implemented by a retroreflector mounted on a delay stage. The delay time of the two optical pulses is much lower than the repetition rate of the laser ($\approx$ 2 us). As a consequence, two photoelectrons generated by two separate laser pulses and two photoelectrons generated by the same pulse are both detected as two-electron events.

As the optical power on the laser tip oscillates for small delay times due to constructive and destructive interference of the laser, the number of generated electrons will strongly vary in this delay regime. Therefore, we selected delays with approximately the same one-electron-state rate ($\pm\sigma/2$) over the integration time of five seconds.

ACKNOWLEDGEMENTS

We thank the members of the Göttingen UTEM team for constant support and useful discussions.
Funding Information: The work at the Göttingen UTEM Lab was funded by the Deutsche Forschungsgemeinschaft (DFG, German Research Foundation) through 432680300/SFB 1456 (project C01) and the Gottfried Wilhelm Leibniz program.
Author contribution: R.H.: Data curation, Formal Analysis, Investigation, Resources, Software, Visualization, Writing - original draft, Writing – review & editing. A.F.: Conceptualization, Formal Analysis, Investigation, Resources, Software, Supervision, Writing - original draft, Writing – review & editing. T.D.: Investigation (supportive), Resources, Software, Visualization, Writing – review & editing. M.M.: Investigation (supportive) Resources, Software, Writing – review & editing. S.V.Y: Methodology, Software, Writing – review & editing. C.R.: Conceptualization, Formal Analysis, Funding acquisition, Methodology, Project administration, Software, Supervision, Visualization, Writing original draft, Writing – review & editing.

* armin.feist@mpinat.mpg.de
† claus.ropers@mpinat.mpg.de

[1] H. Boersch, Z. Physik **139**, 115 (1954).
[2] M. Kuwahara, Y. Nambo, K. Aoki, K. Sameshima, X. Jin, T. Ujihara, H. Asano, K. Saitoh, Y. Takeda, and N. Tanaka, Appl. Phys. Lett. **109**, 013108 (2016).
[3] K. Loeffler, Z. Angew. Phys. **27**, 145 (1969).
[4] G. Jansen, Nuclear Instruments and Methods in Physics Research Section A: Accelerators, Spectrometers, Detectors and Associated Equipment **298**, 496 (1990).
[5] B. Cook, T. Verduin, C. W. Hagen, and P. Kruit, J. Vac. Sci. Technol. B **28**, C6C74 (2010).
[6] N. Bach, T. Domröse, A. Feist, T. Rittmann, S. Strauch, C. Ropers, and S. Schäfer, Struct. Dyn. **6**, 014301 (2019).
[7] B. J. Siwick, J. R. Dwyer, R. E. Jordan, and R. J. D. Miller, J. Appl. Phys. **92**, 1643 (2002).
[8] S. Collin, M. Merano, M. Gatri, S. Sonderegger, P. Renucci, J.-D. Ganière, and B. Deveaud, Journal of Applied Physics **98**, 094910 (2005).
[9] A. M. Michalik and J. E. Sipe, Journal of Applied Physics **99**, 054908 (2006).
[10] B. W. Reed, Journal of Applied Physics **100**, 034916 (2006).
[11] A. Paarmann, M. Gulde, M. Müller, S. Schäfer, S. Schweda, M. Maiti, C. Xu, T. Hohage, F. Schenk, C. Ropers, and R. Ernstorfer, J. Appl. Phys. **112**, 113109 (2012).
[12] B. Cook and P. Kruit, Appl. Phys. Lett. **109**, 151901 (2016).
[13] A. Feist, N. Bach, N. Rubiano da Silva, T. Danz, M. Möller, K. E. Priebe, T. Domröse, J. G. Gatzmann, S. Rost, J. Schauss, S. Strauch, R. Bormann, M. Sivis, S. Schäfer, and C. Ropers, Ultramicroscopy **176**, 63 (2017).
[14] I. Hofmann, *Space Charge Physics for Particle Accelerators*, Particle Acceleration and Detection (Springer International Publishing, Cham, 2017).
[15] P. Emma, Z. Huang, K.-J. Kim, and P. Piot, Phys. Rev. ST Accel. Beams **9**, 100702 (2006).
[16] H. Kiesel, A. Renz, and F. Hasselbach, Nature **418**, 392 (2002).
[17] M. Kuwahara, Y. Yoshida, W. Nagata, K. Nakakura, M. Furui, T. Ishida, K. Saitoh, T. Ujihara, and N. Tanaka, Phys. Rev. Lett. **126**, 125501 (2021).
[18] S. Keramati, W. Brunner, T. J. Gay, and H. Batelaan, Phys. Rev. Lett. **127**, 180602 (2021).
[19] T. Kodama and N. Osakabe, Microscopy **68**, 133 (2019).
[20] P. Hommelhoff, Y. Sortais, A. Aghajani-Talesh, and M. A. Kasevich, Phys. Rev. Lett. **96**, 077401 (2006).
[21] C. Ropers, D. R. Solli, C. P. Schulz, C. Lienau, and T. Elsaesser, Phys. Rev. Lett. **98**, 043907 (2007).
[22] B. Barwick, C. Corder, J. Strohaber, N. Chandler-Smith, C. Uiterwaal, and H. Batelaan, New J. Phys. **9**, 142 (2007).
[23] M. Krüger, M. Schenk, and P. Hommelhoff, Nature **475**, 78 (2011).
[24] G. Herink, D. R. Solli, M. Gulde, and C. Ropers, Nature **483**, 190 (2012).
[25] M. F. Ciappina, J. A. Pérez-Hernández, A. S. Landsman, W. A. Okell, S. Zherebtsov, B. Förg, J. Schötz, L. Seiffert, T. Fennel, T. Shaaran, T. Zimmermann, A. Chacón, R. Guichard, A. Zaïr, J. W. G. Tisch, J. P. Marangos, T. Witting, A. Braun, S. A. Maier, L. Roso, M. Krüger, P. Hommelhoff, M. F. Kling, F. Krausz, and M. Lewenstein, Rep. Prog. Phys. **80**, 054401 (2017), arXiv:1607.01480.
[26] L. Seiffert, T. Paschen, P. Hommelhoff, and T. Fennel, J. Phys. B At. Mol. Opt. Phys. **51**, 134001 (2018).
[27] P. Dombi, Z. Pápa, J. Vogelsang, S. V. Yalunin, M. Sivis, G. Herink, S. Schäfer, P. Groß, C. Ropers, and C. Lienau, Rev. Mod. Phys. **92**, 025003 (2020).
[28] F. Houdellier, G. Caruso, S. Weber, M. Kociak, and A. Arbouet, Ultramicroscopy **186**, 128 (2018).
[29] H. Yanagisawa, S. Schnepp, C. Hafner, M. Hengsberger, D. E. Kim, M. F. Kling, A. Landsman, L. Gallmann, and J. Osterwalder, Sci Rep **6**, 35877 (2016).
[30] A. A. Ischenko, I. V. Kochikov, and R. J. D. Miller, J. Chem. Phys. **150**, 054201 (2019).
[31] J. Schötz, L. Seiffert, A. Maliakkal, J. Blöchl, D. Zimin, P. Rosenberger, B. Bergues, P. Hommelhoff, F. Krausz, T. Fennel, and M. F. Kling, Nanophotonics **10**, 3769 (2021).
[32] S. Meier and P. Hommelhoff, ACS Photonics , acsphotonics.2c00839 (2022).
[33] R. Dörner, V. Mergel, O. Jagutzki, L. Spielberger, J. Ullrich, R. Moshammer, and H. Schmidt-Böcking, Physics Reports **330**, 95 (2000).
[34] J. Ullrich, R. Moshammer, A. Dorn, R. D rner, L. P. H. Schmidt, and H. Schmidt-B cking, Rep. Prog. Phys. **66**, 1463 (2003).
[35] M. Muñoz-Navia, C. Winkler, R. Patel, M. Birke, F. O. Schumann, and J. Kirschner, J. Phys.: Condens. Matter **21**, 355003 (2009).
[36] A. Trützschler, M. Huth, C.-T. Chiang, R. Kamrla, F. O. Schumann, J. Kirschner, and W. Widdra, Phys. Rev. Lett. **118**, 136401 (2017).
[37] S. Larochelle, A. Talebpour, and S. L. Chin, J. Phys. B: At. Mol. Opt. Phys. **31**, 1201 (1998).
[38] W. Becker, X. Liu, P. J. Ho, and J. H. Eberly, Rev. Mod. Phys. **84**, 1011 (2012).
[39] D. Jannis, K. Müller-Caspary, A. Béché, A. Oelsner, and J. Verbeeck, Appl. Phys. Lett. **114**, 143101 (2019).
[40] N. Varkentina, Y. Auad, S. Y. Woo, A. Zobelli, J.-D. Blazit, X. Li, M. Tencé, K. Watanabe, T. Taniguchi, O. Stéphan, M. Kociak, and L. H. G. Tizei, arXiv:2202.12520 (2022), arXiv:2202.12520.
[41] A. Feist, G. Huang, G. Arend, Y. Yang, J.-W. Henke, A. S. Raja, F. J. Kappert, R. N. Wang, H. Lourenço-Martins, Z. Qiu, J. Liu, O. Kfir, T. J. Kippenberg, and C. Ropers, Science **377**, 777 (2022).
[42] O. Kfir, V. Di Giulio, F. J. G. de Abajo, and C. Ropers, Sci. Adv. **7**, eabf6380 (2021).
[43] S. Asban and F. J. García de Abajo, npj Quantum Inf **7**, 42 (2021).
[44] Z. Zhao, X.-Q. Sun, and S. Fan, Phys. Rev. Lett. **126**, 233402 (2021).
[45] Y. Pan and A. Gover, Phys. Rev. A **99**, 052107 (2019).
[46] A. Ben Hayun, O. Reinhardt, J. Nemirovsky, A. Karnieli, N. Rivera, and I. Kaminer, Sci. Adv. **7**, eabe4270 (2021).
[47] D. Rätzel, D. Hartley, O. Schwartz, and P. Haslinger, Phys. Rev. Research **3**, 023247 (2021).
[48] V. Di Giulio, M. Kociak, and F. J. G. de Abajo, Optica

6, 1524 (2019), arXiv:1905.06887.
[49] M. Tsarev, A. Ryabov, and P. Baum, Phys. Rev. Lett. **127**, 165501 (2021).
[50] O. Kfir, Phys. Rev. Lett. **123**, 103602 (2019).
[51] A. Konečná, F. Iyikanat, and F. J. G. de Abajo, ArXiv220200604 Quant-Ph (2022), arXiv:2202.00604 [quant-ph].
[52] N. Rivera and I. Kaminer, Nat Rev Phys **2**, 538 (2020).
[53] B. Cook, M. Bronsgeest, K. Hagen, and P. Kruit, Ultramicroscopy **109**, 403 (2009).
[54] M. S. Bronsgeest, *Physics of Schottky Electron Sources.*, Ph.D. thesis, TU Delft (2009).
[55] A. Bahm, G. Schwind, and L. Swanson, Journal of Applied Physics **110**, 054322 (2011).
[56] T. Kodama, N. Osakabe, and A. Tonomura, Phys. Rev. A **83**, 063616 (2011).
[57] G. Baym and K. Shen, arXiv:1212.4008 (2012), arXiv:1212.4008.
[58] G. van Riessen, Z. Wei, R. S. Dhaka, C. Winkler, F. O. Schumann, and J. Kirschner, J. Phys.: Condens. Matter **22**, 092201 (2010).
[59] D. N. Fittinghoff, P. R. Bolton, B. Chang, and K. C. Kulander, Phys. Rev. Lett. **69**, 2642 (1992).
[60] G. B. Armen, H. Aksela, T. Åberg, and S. Aksela, J. Phys. B: At. Mol. Opt. Phys. **33**, R49 (2000).
[61] S. A. Sheinerman and V. Schmidt, J. Phys. B: At. Mol. Opt. Phys. **30**, 1677 (1997).
[62] Y. Alhassid, Rev. Mod. Phys. **72**, 895 (2000).
[63] O. L. Krivanek, J. P. Ursin, N. J. Bacon, G. J. Corbin, N. Dellby, P. Hrncirik, M. F. Murfitt, C. S. Own, and Z. S. Szilagyi, Phil. Trans. R. Soc. A. **367**, 3683 (2009).
[64] van Schayck, J. Paul, M4I-nanoscopy/tpx3HitParser: Version 2.1.0, Zenodo (2021).
[65] J. P. van Schayck, E. van Genderen, E. Maddox, L. Roussel, H. Boulanger, E. Fröjdh, J.-P. Abrahams, P. J. Peters, and R. B. Ravelli, Ultramicroscopy **218**, 113091 (2020).